EurJIC European Journal of Inorganic Chemistry

ChemPubSoc Europe

FULL PAPER

DOI:10.1002/ejic.201300020

Investigations on the Phase Transition between CdV_2O_6 and $Cd_2V_2O_7$ and Their Photocatalytic Performances

Di Li,[a,b] Xiaojuan Bai,[a] Chengsi Pan,[c] and Yongfa Zhu*[a]

Keywords: Hydrothermal synthesis / Phase transitions / Vanadates / Cadmium

CdV_2O_6 and $Cd_2V_2O_7$ were successfully synthesized by a simple hydrothermal process. The effects of the hydrothermal temperature and pH on the phase transition between CdV_2O_6 and $Cd_2V_2O_7$ were investigated in detail. That the $Cd_2V_2O_7$ phase could transform into CdV_2O_6 was attributed to polymerization of vanadate in an acidic environment as the V/O ratio increased as the pH decreased. $V_2O_7^{4-}$ was stable in a neutral or alkaline environment at an identical hydrothermal temperature, therefore, the $Cd_2V_2O_7$ phase was obtained after hydrothermal treatment for 24 h. Because the degree of hydrolysis of NH_4Cl increased with increasing temperature in the solution, the increased temperature accelerated the speed of the pH decrease. Therefore, the hydrothermal temperature played an important part in the phase transition between CdV_2O_6 and $Cd_2V_2O_7$. CdV_2O_6 and $Cd_2V_2O_7$ showed high photocatalytic activity for the degradation of methylene blue under visible-light irradiation.

Introduction

Complex vanadium(V) oxides have received renewed interest as electrode materials and catalysts.[1–13] According to a previous theoretical study, the V 3d orbital is usually located below the analogous d orbitals of other transition metals in the energy spectrum, and, therefore, the bottom conduction band is lowered to a more positive position.[14] Accordingly, vanadium is an important candidate element for visible-light photocatalysts. Some vanadium-containing oxides, such as $BiVO_4$ and $InVO_4$, have been developed successfully as visible-light photocatalysts for O_2 and H_2 evolution in the presence of the sacrificial reagents $AgNO_3$ and CH_3OH, respectively.[15,16] Recently, Wang and co-workers found that $Zn_3V_2O_8$ had photocatalytic activity for O_2 evolution under visible-light irradiation.[17] Zhu and co-workers have investigated the hierarchical nanostructure of $Zn_3V_2O_7(OH)_2(H_2O)_2$ with flowerlike and nanobelt morphologies and converted the $Zn_3V_2O_7(OH)_2(H_2O)_2$ precursors into porous $Zn_3V_2O_8$.[18] They found that the photocatalytic activities were significantly improved when $Zn_3V_2O_8$ had a flower-shaped superstructure. However, work concerning the phase transition between CdV_2O_6 and $Cd_2V_2O_7$ under hydrothermal conditions has not been reported. No work has been reported on CdV_2O_6 and $Cd_2V_2O_7$ as photocatalysts. Therefore, there is a need to investigate the phase-transition mechanism of CdV_2O_6 and $Cd_2V_2O_7$ and their photocatalytic activity.

In this paper, CdV_2O_6 and $Cd_2V_2O_7$ were controllably synthesized by a simple hydrothermal method. The influence of the reaction parameters (pH and hydrothermal temperature) on the phase transition between CdV_2O_6 and $Cd_2V_2O_7$ and the relationship between the phases and photocatalytic activities were investigated. The formation of CdV_2O_6 and $Cd_2V_2O_7$ depended on the pH under identical hydrothermal temperatures. The hydrolysis of NH_4Cl played an important part in the formation of CdV_2O_6 and $Cd_2V_2O_7$ under different hydrothermal temperatures. CdV_2O_6 and $Cd_2V_2O_7$ showed highly efficient photocatalytic activities for the photocatalytic decomposition of methylene blue (MB).

Results and Discussion

Controlled Synthesis of CdV_2O_6 and $Cd_2V_2O_7$

The pH of the precursor precipitates had a crucial effect on the formation of CdV_2O_6 and $Cd_2V_2O_7$. The precursor suspensions were adjusted to the desired pH by adding NaOH and HCl solutions and then they were hydrothermally treated at 180 °C for 24 h. Figure 1 shows the XRD patterns of CdV_2O_6 and $Cd_2V_2O_7$ samples prepared by hydrothermal synthesis at different pH values. At pH 6, the diffraction peaks of all the samples were easily indexed as a pure, orthorhombic crystalline phase CdV_2O_6, which is in good agreement with the standard card (JCPDS Card

[a] Department of Chemistry, Tsinghua University, Beijing 100084, China
Fax: +86-10-6278-7601
E-mail: zhuyf@mail.tsinghua.edu.cn
Homepage: http://www.tsinghua.edu.cn/publish/index.html
[b] School of Metallurgical Engineering, Xi'an University of Architecture and Technology, Xi'an 710055, People's Republic of China
[c] Department of Chemical System Engineering, The University of Tokyo, 7-3-1 Hongo, Bunkyo-ku, Tokyo 113-8656, Japan

Supporting information for this article is available on the WWW under http://dx.doi.org/10.1002/ejic.201300020.

number: 20-0189). At pH 7 or 8, the product was pure $Cd_2V_2O_7$, which was in good agreement with the standard card (JCPDS Card number: 78-0951). At pH 9 or 5, products that contained other phase were obtained. The microstructures of the as-prepared samples were investigated with scanning electron microscopy (SEM). Figure 2 (a) shows an SEM micrograph of CdV_2O_6 prepared at pH 6, from which one can see that the sample is made up of short, thick rods. At pH 7 and 8, particles were observed in the SEM micrograph of $Cd_2V_2O_7$ (Figure 2, b–d), and it appeared that the particles increased in size as pH value increased.

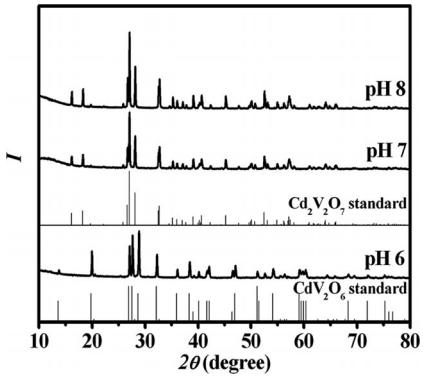

Figure 1. XRD patterns samples at different pH values treated at 180 °C.

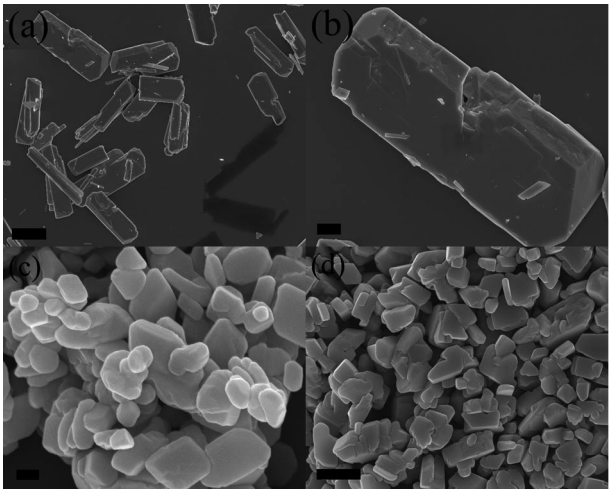

Figure 2. Morphologies of samples at different values treated at 180 °C: (a) and (b) pH 6, (c) pH 7, and (d) pH 8. The scale bar is 10 μm in (a), 2 μm in (b), 200 nm in (c), and 1 μm in (d).

Formation Mechanism of CdV_2O_6 and $Cd_2V_2O_7$

The formation of CdV_2O_6 rods is a typical hydrothermal phase-transition process: a highly supersaturated solution was adopted, and hollow spherical particles acted as the precursor for the synthesis of crystalline $Cd_2V_2O_7$ particles. It appeared that the $Cd_2V_2O_7$ particles accumulated by self-assembly. At the beginning, the direct mixing of the two solutions at pH 6 led to the formation of a lot of hollow spherical particles (Figure 3, a and b). Upon hydrothermal treatment, the $Cd_2V_2O_7$ phase transformed to α-CdV_2O_6, which is in good agreement with the standard card (JCPDS Card number: 73-0187). The $Cd_2V_2O_7$ phase transformed to α-CdV_2O_6 because of the polymerization of vanadate in an acidic environment, and the V/O ratio increased as the pH decreased.[19–21] Finally, the α-CdV_2O_6 phase transformed to CdV_2O_6, which means that CdV_2O_6 is the thermodynamically stable phase (Figure 4).

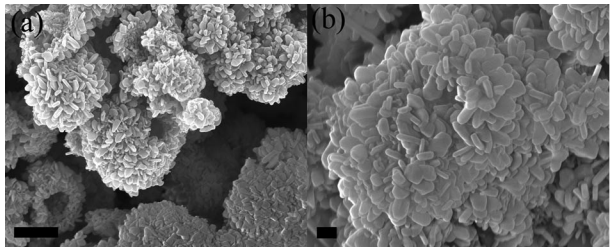

Figure 3. Morphologies of $Cd_2V_2O_7$ synthesized by the direct mixing of NH_4VO_3 and $CdCl_2$ solutions. The scale bar is 1 μm in (a) and 200 nm in (b).

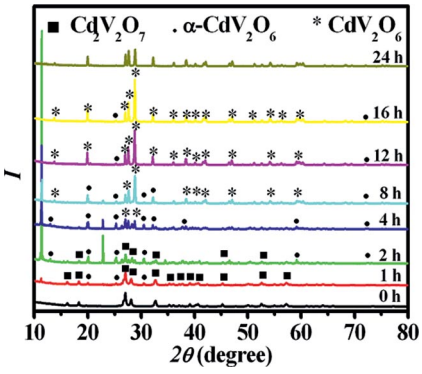

Figure 4. XRD patterns of samples treated for different durations at pH 6 and 180 °C.

Conversely, $Cd_2V_2O_7$ grew by a simple hydrothermal ripening process.[22] Initially, the direct mixing of the two solutions led to the formation of $Cd_2V_2O_7$ hollow spherical particles (Figure 3). At pH 8, the phases became a mixture. Upon hydrothermal treatment, the mixture transformed to a pure $Cd_2V_2O_7$ phase after 4 h (Figure 5). SEM images of a series samples treated at 180 °C for different durations are in accord with the XRD patterns; the $Cd_2V_2O_7$ particles appeared only after 4 h of hydrothermal treatment (Figure 6, a). The particle morphology appeared at the same time as the $Cd_2V_2O_7$ crystalline phase. Under hydrothermal treatment, the formation of tiny crystalline nuclei in a supersaturated medium occurred and was followed by crystal growth. Large particles grow at the cost of small ones because of the energy difference in the solubility between the large and small particles according to the well-known Gibbs–Thomson law.[23] In the early stages, an examination of the intermediate samples showed the coexistence of irregular large particles and nanoparticles (Figure 6, b and c). As the reaction continued, the irregular nanoparticles disappeared, and the large particles increased in size, which suggests that the large particles grew at the cost of the small

particles (Figure 6, d).[24,25] The $Cd_2V_2O_7$ phase did not transform to CdV_2O_6. The $Cd_2V_2O_7$ phase was obtained after hydrothermal treatment for 24 h because $V_2O_7^{4-}$ is stable in a neutral or alkaline environment under identical hydrothermal temperatures.

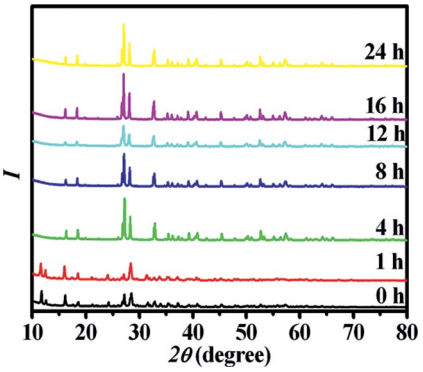

Figure 5. XRD patterns of samples treated for different durations at pH 8 and 180 °C.

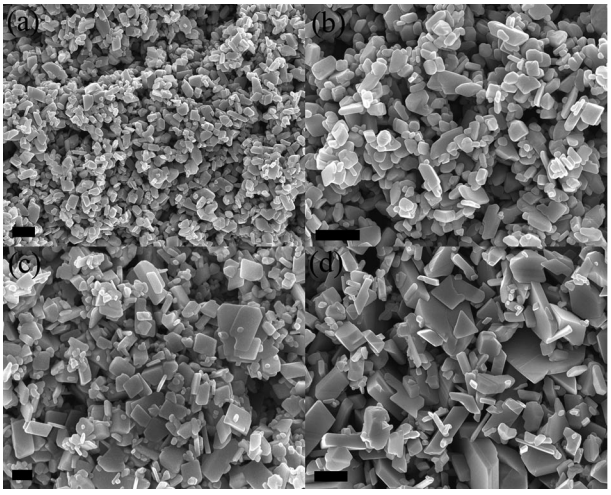

Figure 6. Morphologies of samples treated for different durations at pH 8 and 180 °C: (a) 4 h, (b) 8 h, (c) 12 h, and (d) 16 h. The scale bar is 1 μm in (a), (b), and (d), and 300 nm in (c).

Effects of Temperature on the Formation of CdV_2O_6 and $Cd_2V_2O_7$

The hydrothermal temperature had a significant effect on the formation of CdV_2O_6 and $Cd_2V_2O_7$. Figure 7 shows XRD patterns of samples prepared at various hydrothermal temperatures at pH 6. The product was a mixture of CdV_2O_6, $Cd_2V_2O_7$, and α-CdV_2O_6 after treatment at 120 °C. The amount of CdV_2O_6 formed increased with increasing temperature, and the $Cd_2V_2O_7$ and α-CdV_2O_6 phases were transformed into CdV_2O_6. It appears that the hydrothermal phase-transition process from the CdV_2O_6 rods occurs at 180 °C. This is attributed to the hydrolysis of NH_4Cl, which is an endothermic reaction ($\Delta H > 0$), and we can obtain the formula:

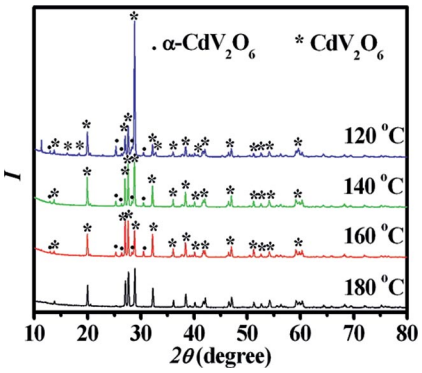

Figure 7. XRD patterns of samples treated at different temperatures at pH 6.

$$\ln\frac{K_2}{K_1}=\frac{\Delta H}{R}\left(\frac{1}{T_1}-\frac{1}{T_2}\right)$$

The hydrolysis constant K_h increased with increasing temperature, so the degree of hydrolysis increased with increasing temperature. The H^+ concentration increased with increasing temperature, which accelerates the rate of the decrease in pH. Therefore, the pure CdV_2O_6 phase was obtained at 180 °C.

Figure 8 shows the XRD patterns of samples prepared at various hydrothermal temperatures at pH 8. At 240 °C, the $Cd_2V_2O_7$ phase began to transform into the CdV_2O_6 phase. The transformation of the $Cd_2V_2O_7$ phase into the CdV_2O_6 phase was also attributed to the hydrolysis of NH_4Cl. As mentioned above, the hydrolysis constant K_h increased with increasing temperature, so the degree of hydrolysis increased with increasing temperature. The concentration of H^+ increased with increasing temperature. At 240 °C, the hydrothermal environment was acidic. Therefore, the $Cd_2V_2O_7$ phase began to transform to the CdV_2O_6 phase.

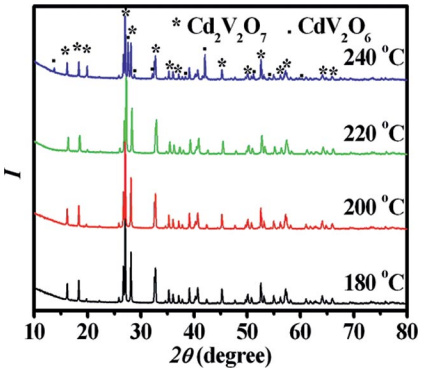

Figure 8. XRD patterns of samples treated at different temperatures at pH 8.

Optical Properties and Photocatalytic Activity

The optical absorption of CdV_2O_6 and $Cd_2V_2O_7$ was measured by using a UV/Vis spectrometer. Figure 9 shows typical diffuse reflection spectra (DRS) of CdV_2O_6 and

$Cd_2V_2O_7$ obtained at different pH values. The steep shape of the spectra indicated that the visible-light absorption was not caused by a transition from the impurity level but was caused by the band-gap transition.[26] The CdV_2O_6 had a wider absorption range, which meant the CdV_2O_6 could absorb more visible light. The optical absorption range of CdV_2O_6 was wider than that of $Cd_2V_2O_7$ because the polymerization degree of vanadate increased as the pH decreased. The vanadate became darker, so the absorption range broadened. The band gap of the sample can be evaluated from the following equation: $\alpha(h\upsilon) = A(h\upsilon - E_g)^{n/2}$, in which α, n, E_g, and A are the absorption coefficient, light frequency, band-gap energy, and a constant, respectively.[27,28] Among them, n depends on the characteristics of the transition in a semiconductor. For CdV_2O_6 and $Cd_2V_2O_7$, the value of n is 1 for the direct transition.[29] The band-gap energy (E_g) of the as-prepared sample can be thus estimated from a plot of $(\alpha h\upsilon)^2$ vs. photon energy ($h\upsilon$). The intercept of the tangent with the x axis gives a good approximation of the band-gap energy for the sample. The inset of Figure 9 shows the plot of $(\alpha h\upsilon)^2$ vs. $h\upsilon$ calculated from the absorption spectrum. Finally, the band-gap energy of the CdV_2O_6 and $Cd_2V_2O_7$ samples are shown in Table 1. The band-gap value of CdV_2O_6 is much lower than that of $Cd2V_2O_7$ because CdV_2O_6 has a wider absorption range. The band-gap value of $Cd_2V_2O_7$ obtained at pH 7 is higher than that of $Cd_2V_2O_7$ obtained at pH 8, because of the size effects of $Cd_2V_2O_7$.[30]

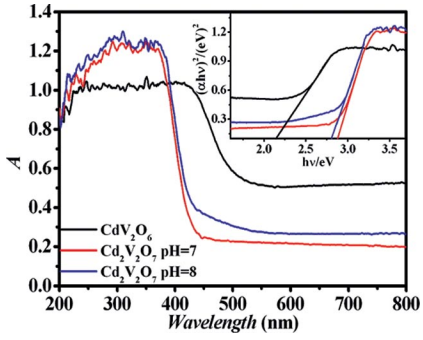

Figure 9. UV/Vis diffuse reflectance spectra of CdV_2O_6 and $Cd_2V_2O_7$ treated at 180 °C. The inset shows the plots of $(\alpha h\upsilon)^2$ vs. photon energy ($h\upsilon$).

Table 1. The direct band gaps calculated from their corresponding absorption spectra for CdV_2O_6 and $Cd_2V_2O_7$ treated at 180 °C.

Sample	CdV_2O_6	$Cd_2V_2O_7$ (pH 7)	$Cd_2V_2O_7$ (pH 8)
Band gap [eV]	2.144	2.878	2.809

Methylene blue (MB) was used as a probe of the heterogeneous photocatalysis of the samples, and the decomposition could be monitored by the visible-light absorption signature. The characteristic absorption of MB at 664 nm was chosen as the monitored parameter for the photocatalytic degradation process. Figure 10 shows plots of the degradation of MB in the presence of CdV_2O_6 and $Cd_2V_2O_7$ pH series samples. A first-order linear relationship was revealed by plots of $\ln(C/C_0)$ vs. irradiation time (t); C is the concentration of MB at the irradiation time t and C_0 is the concentration in the adsorption equilibrium of the photocatalysts before irradiation. From the first-order linear fit, the determined reaction rate constants k were 0.29842, 0.27441, and 0.29897 h^{-1}, respectively, for the CdV_2O_6 and $Cd_2V_2O_7$ pH series samples. Among the $Cd_2V_2O_7$ pH series samples, the photocatalytic activity increased as the pH value increased. As confirmed by the XRD results, the crystallinity of the sample obtained at pH 7 was lower than that at pH 8. The higher crystallinity meant there were fewer defects in the as-synthesized sample. Lattice defects can act as recombination centers for photoinduced electrons and holes and, thus, significantly reduce the photocatalytic activity.[31,32] However, the light absorption intensity also makes a key contribution to the photocatalytic activity.[33] From the DRS spectra in Figure 9, CdV_2O_6 shows much enhanced visible-light absorption intensity over that of $Cd_2V_2O_7$. However, the $Cd_2V_2O_7$ obtained at pH 8 had small crystals with a relatively larger reaction area. Therefore, the photocatalytic activity of $Cd_2V_2O_7$ obtained at pH 8 and CdV_2O_6 was similar.

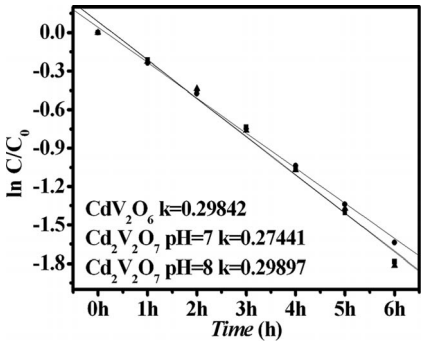

Figure 10. First-order plots of the photocatalytic degradation of MB with samples synthesized at different pH values (squares: CdV_2O_6, circles: $Cd_2V_2O_7$ obtained at pH 7, triangles: $Cd_2V_2O_7$ obtained at pH 8).

Conclusions

CdV_2O_6 and $Cd_2V_2O_7$ were controllably synthesized by a simple hydrothermal method. With hydrothermal treatment, the $Cd_2V_2O_7$ phase was transformed to CdV_2O_6; this was attributed to the polymerization of vanadate in an acid environment. As $V_2O_7^{4-}$ is stable in a neutral or alkaline environment under identical hydrothermal temperature, the $Cd_2V_2O_7$ phase could be obtained in neutral or alkaline environment. However, the $Cd_2V_2O_7$ phase began to transform to the CdV_2O_6 phase in an alkaline environment at 240 °C. This is attributed to the hydrolysis of NH_4Cl. The photocatalytic properties of CdV_2O_6 and $Cd_2V_2O_7$ were investigated under visible-light irradiation. It was found that CdV_2O_6 and $Cd_2V_2O_7$ possessed a high catalytic activity towards the degradation of MB.

Experimental Section

Materials: Analytical reagent grade methylene blue was used without further purification. Other chemicals were commercial products of analytical grade or reagent grade. All solutions were prepared with distilled water.

Preparation of CdV_2O_6 and $Cd_2V_2O_7$: In a typical procedure, NH_4VO_3 (4 mmol) was dissolved in deionized water (14 mL). Under vigorous agitation, an aqueous solution (14 mL) containing $CdCl_2{\cdot}2.5H_2O$ (2 mmol) was added to the above solution at room temperature. The pH value of the mixture was adjusted with 1 M NaOH and HCl (36%). The mixture was then transferred into a 40 mL Teflon-lined steel autoclave. The autoclave was heated under autogenous pressure at a series of temperatures for 24 h. The autoclave was cooled gradually to room temperature. The precipitate was washed with distilled water three times and then dried at 60 °C in air.

Characterizations: The degradation rates of methylene blue (MB) solutions were monitored with a Hitachi U-3010 spectrophotometer, and the maximum absorption wavelength of the MB solutions was identified as 664 nm. The UV/Vis spectra were recorded in the range 200–800 nm. The UV/Vis diffuse reflectance spectra (UV/Vis DRS) of the samples were obtained with a UV/Vis spectrophotometer (UV-3010, Shimadzu) equipped with an integrating-sphere accessory. $BaSO_4$ was used as a reflectance standard. The pH values were measured with a PHSJ-4A pH meter. XRD experiments were performed with a Rigaku DMAX-2400 diffractometer with Cu-K_α radiation. The size and morphologies of CdV_2O_6 and $Cd_2V_2O_7$ were characterized with the aid of a LEO-1530 field emission scanning electron microscope (SEM).

Photocatalytic Oxidative Degradation: The photocatalytic activities of CdV_2O_6 and $Cd_2V_2O_7$ were evaluated by the decomposition of MB under visible-light irradiation. A 500 W xenon lamp ($\lambda >$ 290 nm, Institute of Electric Light Sources, Beijing) was focused through a window, and a 420 or 450 nm cutoff filter was placed onto the cell window to ensure the desired irradiation conditions. The average light intensity was 40 mW cm^{-2}. The radiant flux was measured with a power meter (Institute of Electric Light Sources, Beijing).

A cylindrical double-layer glass photochemical reactor with internal diameter 70 mm, external diameter 80 mm, and height 80 mm was utilized for the photocatalysis reactions. A distance of about 12 cm between the lamp and reactor was maintained. Running water was piped into the layer to keep the temperature constant.

The photocatalytic degradation of MB in the aqueous solutions was studied by using CdV_2O_6 or $Cd_2V_2O_7$ as the photocatalyst at room temperature and normal atmospheric pressure. CdV_2O_6 or $Cd_2V_2O_7$ (50 mg) and an MB aqueous solution (100ml, 1×10^{-5} M) were added to the reactor. The mixture was stirred with a magnetic stirrer prior to irradiation with a xenon lamp at room temperature. Prior to irradiation, the solution was kept in the dark for 60 min to ensure the equilibrium of the working solution. After the reaction, the sample solution was put in a centrifuge to remove CdV_2O_6 or $Cd_2V_2O_7$ from the solution. The solution obtained this way was extracted into a quartz cell. The absorbance of the samples was measured with quartz cells every 60 min.

Calculation Approach: The hydrolysis constant of NH_4Cl (K_h) can be calculated from following formula: $K_h = K_w/K_b$, where K_w is the ion product constant of water and K_b is the equilibrium dissociation constant of ammonia.

Supporting Information (see footnote on the first page of this article): C/C_0-time plots of the photocatalytic degradation of MB and MB solution with CdV_2O_6 in the dark.

Acknowledgments

This work was supported by the Chinese National Science Foundation (NSFC) (grant numbers 20925725 and 50972070), the National High Technology Research and Development Program of China (grant number 2012AA062701), and the Tsinghua University Initiative Scientific Research Program.

[1] A. Kudo, K. Omori, H. Kato, *J. Am. Chem. Soc.* **1999**, *121*, 11459–11467.
[2] S. Kohtani, M. Koshiko, A. Kudo, K. Tokumura, Y. Ishigaki, A. Toriba, K. Hayakawa, R. Nakagaki, *Appl. Catal. B* **2003**, *46*, 573–586.
[3] J. Ye, Z. Zou, M. Oshikiri, A. Matsushita, M. Shimoda, M. Imai, T. Shishido, *Chem. Phys. Lett.* **2002**, *356*, 221–226.
[4] Z. Zou, J. Ye, K. Sayama, H. Arakawa, *Chem. Phys. Lett.* **2001**, *343*, 303–308.
[5] Z. Zou, J. Ye, K. Sayama, H. Arakawa, *Chem. Phys. Lett.* **2001**, *333*, 57–62.
[6] Y. T. Yeom, S. H. Choh, M. L. Du, M. S. Jang, *Phys. Rev. B* **1996**, *53*, 3415–3421.
[7] K. Hirota, G. Komatsu, M. Yamashita, H. Takemura, O. Yamaguchi, *Mater. Res. Bull.* **1992**, *27*, 823–830.
[8] K. Sayama, A. Nomura, Z. G. Zou, R. Abe, Y. Abe, H. Arakawa, *Chem. Commun.* **2003**, 2908–2909.
[9] Y. Zhao, Y. Xie, X. Zhu, S. Yan, S. X. Wang, *Chem. Eur. J.* **2008**, *14*, 1601–1606.
[10] D. Ke, T. Peng, L. Ma, P. Cai, K. Dai, *Inorg. Chem.* **2009**, *48*, 4685–4691.
[11] S. Tokunaga, H. Kato, A. Kudo, *Chem. Mater.* **2001**, *13*, 4624–4628.
[12] J. S. Li, D. Q. Zhang, J. C. Yu, *Chem. Mater.* **2008**, *20*, 3983–3992.
[13] G. Xi, J. Ye, *Chem. Commun.* **2010**, *46*, 1893–1895.
[14] M. Oshikiri, M. Boero, J. Ye, Z. Zou, G. Kido, *J. Chem. Phys.* **2002**, *117*, 7313–7318.
[15] J. Yu, A. Kudo, *Adv. Funct. Mater.* **2006**, *16*, 2163–2169.
[16] J. Ye, Z. Zou, M. Oshikiri, A. Matsushita, M. Shimoda, M. Imai, T. Shishido, *Chem. Phys. Lett.* **2002**, *356*, 221–226.
[17] D. Wang, J. Tang, Z. Zou, J. Ye, *Chem. Mater.* **2005**, *17*, 5177–5182.
[18] R. Shi, Y. Wang, F. Zhou, Y. Zhu, *J. Mater. Chem.* **2011**, *21*, 6313–6320.
[19] J. Muster, G. T. Kim, V. Krstic, J. G. Park, M. Burghard, *Adv. Mater.* **2000**, *12*, 420–424.
[20] J. F. Jiu, X. Wang, Q. Peng, Y. D. Li, *Adv. Mater.* **2005**, *17*, 764–767.
[21] D. Errandonea, R. S. Kumar, S. N. Achary, O. Gomis, F. J. Manjón, R. Shukla, A. K. Tyagi, *J. Appl. Phys.* **2012**, *111*, 053519.
[22] S. H. Yu, B. Liu, M. S. Mo, J. H. Huang, X. M. Liu, Y. T. Qian, *Adv. Funct. Mater.* **2003**, *13*, 639–647.
[23] J. W. Mullin, *Crystallization*, 3rd ed., Butterworth–Heinemann, Oxford, UK, **1997**.
[24] C. B. Murray, D. J. Norris, M. G. Bawendi, *J. Am. Chem. Soc.* **1993**, *115*, 8706–8715.
[25] H. Zhang, L. Wang, H. Xiong, L. Hu, B. Yang, W. Li, *Adv. Mater.* **2003**, *15*, 1712–1715.
[26] A. Kudo, I. Tsuji, H. Kato, *Chem. Commun.* **2002**, 1958–1959.
[27] X. Zhang, Z. H. Ai, F. L. Jia, L. Z. Zhang, *J. Phys. Chem. C* **2008**, *112*, 747–753.
[28] X. Xiao, W. Zhang, *RSC Adv.* **2011**, *1*, 1099–1105.

[29] V. Panchal, D. Errandonea, A. Segura, P. Rodríguez-Hernandez, A. Muñoz, S. Lopez-Moreno, M. Bettinelli, *J. Appl. Phys.* **2011**, *110*, 043723.
[30] A. L. Linsebigler, G. Lu, J. T. Yates Jr., *Chem. Rev.* **1995**, *95*, 735–758.
[31] J. B. Mu, C. L. Shao, Z. C. Guo, M. Y. Zhang, Z. Y. Zhang, P. Zhang, B. Chen, Y. C. Liu, *J. Mater. Chem.* **2012**, *22*, 1786–1793.
[32] Y. W. Wang, L. Z. Zhang, K. J. Deng, X. Y. Chen, Z. G. Zou, *J. Phys. Chem. C* **2007**, *111*, 2709–2714.
[33] N. Zhang, S. Liu, X. Fu, Y. Xu, *J. Phys. Chem. C* **2011**, *115*, 9136–9145.

Received: January 8, 2013
Published Online: April 22, 2013

